Probing the Spatial Distribution and Morphology of Supported Nanoparticles Using Rutherford-Scattered Electron Imaging**

Paul A. Midgley,* Matthew Weyland, John Meurig Thomas,* Pratibha L. Gai,* and Edward D. Boyes

There is a growing need for ultrasensitive methods that can determine the size, elemental composition, precise location, spatial distribution, and detailed morphology of a wide variety of nanoparticles anchored on high-area supports. In the field of heterogeneous catalysis alone, and in the related area of fuel-cell technology, many different high-area (and generally low-atomic-number, Z) supports such as silica, alumina, and magnesia, as well as graphitic, amorphous, or adamantine carbons and thermally stable polymers, are employed. The active nanoparticles consist almost invariably of either pure, high-Z elements such as Pt, Pd, and Ru, or heterometallic species such as Pt–Pd, Pt–Fe, Pt–Cu, Pt–Ru, or Pt–Fe–Co, Pt–Cr–Co, and Pt–Co–Ga.[1–7] In the field of constrained colloidal and metal clusters which exhibit electronic quantum size effects, typical nanoparticle materials are CdS, CdSe, and Cd_3P_2.[1,8,9] There are, in addition, many other areas of nanotechnology and biology where it is important to obtain three-dimensional (3D) morphological information, as well as knowledge of the spatial distribution and composition of nanoparticles.

It has been shown previously that the size and distribution of minute particles of the kind described above are conveniently investigated using high-resolution scanning transmission electron microscopy (STEM) equipped with a high-angle annular dark-field (HAADF) detector.[10–14] To a good approximation, electrons scattered at high angles (greater than 30 mrad) obey Rutherford's scattering law: that the scattering cross-section is proportional to Z^2. Moreover, the scattered electron wave is predominantly incoherent in nature, so that images formed using a HAADF "Rutherford" detector do not show the complicating contrast changes associated with coherent scattering, such as those which occur in bright-field (BF) images (formed from Bragg-scattered electrons). As a consequence, HAADF images can be interpreted directly and their intensity is a monotonic function of the sample thickness and atomic number, which is a prerequisite for the electron tomography experiments described below.

Back-scattered electrons (BSEs), which are those electrons scattered to angles greater than 90° (see Figure 1), also yield sharp images for nanoparticles that contain more than 100 atoms of high-Z materials distributed over low-Z supports, because they too obey Rutherford's scattering law. BSE scattering may be thought of as "reverse Rutherford scattering" although the exact form of the experimental BSE scattering is modified by the high (greater than 90°) scattering angle and by the bulk specimen environment.[15–17] Figure 2 shows typical examples of Rutherford-scattered imaging of nanoparticles of a commercially important palladium-on-carbon catalyst recorded with a BSE detector in a field-emission scanning electron microscope (a), as well as a STEM HAADF image of the same sample (b), recorded in the same instrument. It is clear that high spatial resolution (of the order of 1 nm) is achievable by scanning electron microscopy (SEM), which was performed at 30 kV, and that similar images are obtained in either back-scattered (BSE) or forward-scattered (HAADF) mode. It is a simple matter to identify small particles in thin sections by energy dispersive X-ray (EDX) methods. With a bulk (electron-opaque) sample the sensitivity of the BSE method in the nanometer range, and of EDX on the submicron scale, increases at medium-to-low voltages (limited by instrumental parameters). The mixing of the SEM BSE signal, primarily for higher-Z particle imaging, with a component of secondary-electron imaging, for lower-Z support topography, together with the use of medium-to-low

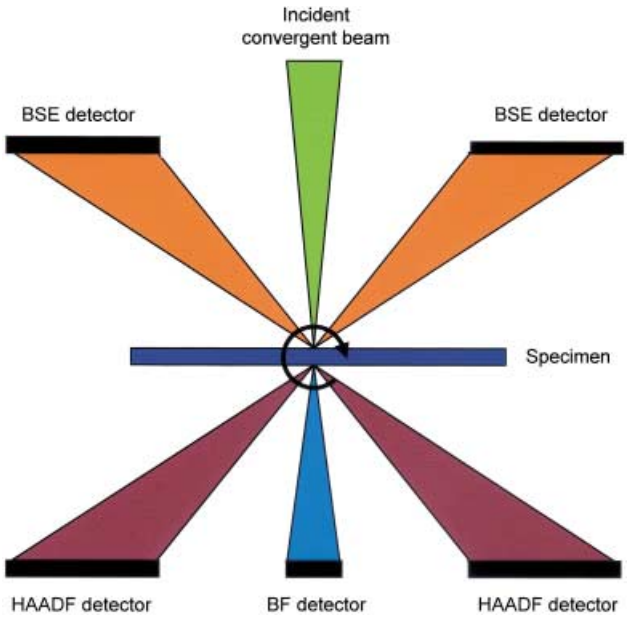

Figure 1. Schematic diagram illustrating the geometry of detectors used for STEM BF, STEM HAADF, and SEM BSE imaging.

[*] Dr. P. A. Midgley, Prof. Sir J. M. Thomas, Dr. M. Weyland
Department of Materials Science and Metallurgy
University of Cambridge
Pembroke Street, Cambridge, CB2 3QZ (UK)
Fax: (+44) 1223-334-567
E-mail: pam33@cam.ac.uk
dawn@ri.ac.uk
Prof. Sir J. M. Thomas
Davy-Faraday Research Laboratory
Royal Institution of Great Britain
21 Albermarle Street, London, W1X 4BS (UK)
Fax: (+44) 207-670-2988
Dr. P. L. Gai,[+] Dr. E. D. Boyes
DuPont, Central Research and Development
Wilmington, DE 19880-0356 (USA)
[+] Also at:
University of Delaware
Department of Materials Science and Engineering
Newark, DE (USA)

[**] We gratefully acknowledge the support (by a rolling grant to J.M.T. and joint grants to P.A.M. and J.M.T.) by the EPSRC (UK) and the Royal Commission for the Exhibition of 1851 for a Fellowship (to M.W.).

  0044-8249/02/4120-3804 $ 20.00+.50/0

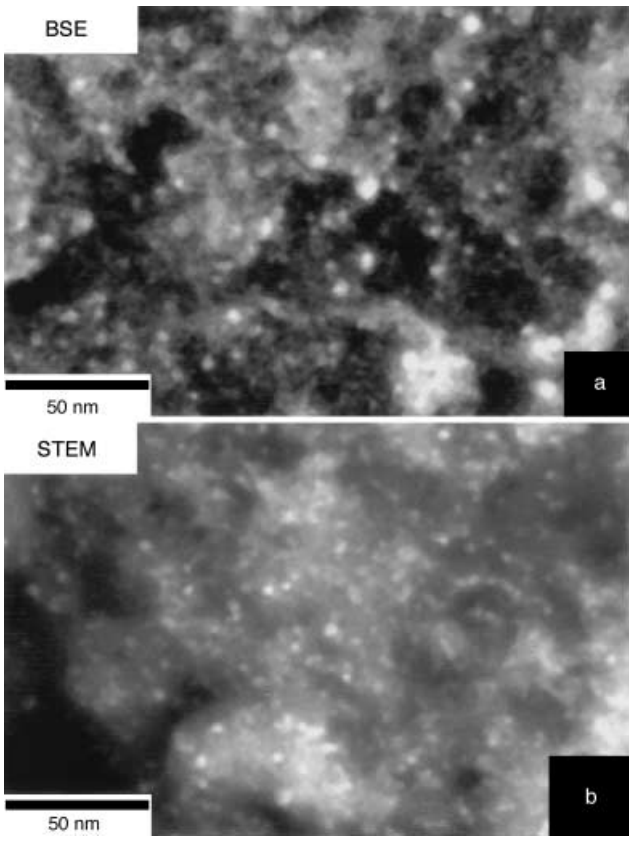

Figure 2. a) SEM BSE image and b) STEM HAADF image of Pd nanoparticles supported on a semicrystalline carbon support.

beam energies, may prove to be the optimum combination for SEM imaging.[18]

Since the late 1960's,[19,20] electron tomography has been used in the biological sciences to investigate the 3D structure of both highly symmetric objects (for example, viruses and macromolecules) as well as those lacking crystallographic (or other) order (for example, cells). However, it is only very recently that this approach has been applied successfully by de Jong, Koster, and co-workers[21,22] to the study of physical systems, in particular zeolitic materials, using conventional BF (Bragg-scattering) transmission electron microscopy (TEM) imaging.

For electron tomography, a series of images must be recorded at successive tilt angles using a signal that satisfies the "projection requirement", namely that the signal used to form the images must be a monotonic function of the projected thickness of the object under study.[19,23] For a crystalline object, the diffraction contrast prevalent in a BF image generally rules out such images for tomographic use. Furthermore, if a coherent (or even partially coherent) beam is used, as is the case in most modern field-emission electron microscopes, the images of even non-crystalline objects may show Fresnel fringes, the intensities of which will also not satisfy the projection requirement.[24]

High-angle-scattered electrons, recorded by STEM with a HAADF detector and SEM with a BSE detector, offer an essentially incoherent signal that does satisfy the projection requirement, even for crystalline objects. Firstly, such images are monotonically dependent on the atomic number of the object and its thickness. The strong Z-dependence can be seen from Figure 2: the "heavy" (high-Z) nanoparticles stand out clearly from the semicrystalline carbon support. The clarity of the image is testimony to the superiority of the HAADF and BSE approach over either BF STEM or BF TEM for imaging these structures. Secondly, the large beam currents used in fixed-beam methods (e.g. conventional TEM) can very rapidly damage any material that is beam-sensitive; many catalyst systems fall into this category. However, in STEM and BSE SEM, a much smaller degree of beam exposure is involved. Although the current density within the convergent probe is high, its energy can be dissipated to the surrounding (non-illuminated) areas. In addition, it is possible to minimise ionisation damage by changing the operating voltage in the STEM to a high voltage (300 kV) which reduces the inelastic scattering cross-section.

We turn now to the results from the sample of the commercial 5 % Pd/C catalyst. Figure 3 a shows a single raw image from a series of HAADF images taken using a Philips CM300 field-emission gun (FEG) (S)TEM apparatus at successive tilt angles from $+60$ to $-54°$. A modified high-tilt holder allows us to go beyond the manufacturer's limits.[25] Figure 3 b shows a selection of images of the same specimen where each image is now a projection of the reconstructed 3D structure (at the stipulated angles).[26] The reconstruction was obtained by using an iterative back-projection approach;[22,27–30] the concept of back-projection is shown schematically in Figure 4. The wealth of retrievable information pertaining to the nature of this supported catalyst from the electron-tomographic (Z-contrast) method is unprecedented. It is clear that the original image has a better spatial resolution than the reconstruction. This is primarily because the overall resolution is limited by the field depth. The object is about 600 nm in diameter and so, from previous work,[27] we would expect a spatial resolution of about 6 nm in all directions, even though the resolution in a single original image is nominally about 1 nm. The loss of resolution, particularly in the direction parallel to the optic axis of the microscope, is brought about by the missing "wedge" of data resulting from the limited tilt range. Despite this loss of resolution, it is obvious that this is a powerful high-resolution technique for monitoring progressive changes in the 3D distribution and attributes of supported nanoparticles and their use as catalysts.

We have shown that the STEM method of probing materials can be complemented with field-emission SEM. The resolution achievable with these instruments is such that the ability to locate the position (and determine the composition) of nanoparticles anchored at the surface (or buried just beneath the surface) of supports, is very considerable (see Figure 2). A comparison of HAADF and BSE images of a commercial 5 % Pd/C system has shown that BSE imaging can be a simple and effective method in the study of surface-loaded nanocatalysts. BSE imaging does not require electron transparency through the support, in contrast to TEM or STEM analysis. This will allow access to larger (mm scale) support units, as will often be the case in many industrial applications, although by its nature it will primarily reveal distributions at the surface, and not deep within any support-

  0044-8249/02/4120-3805 $ 20.00+.50/0

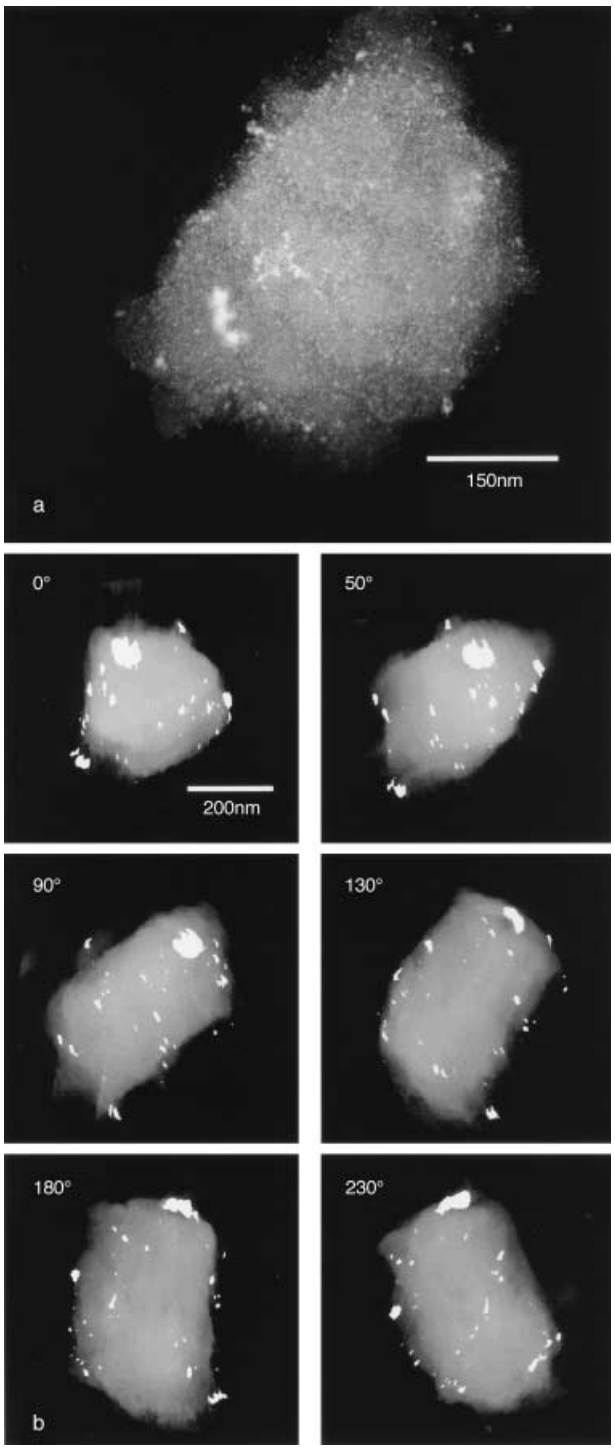

Figure 3. a) A STEM HAADF image acquired from the same Pd/C sample as shown in Figure 2. The large difference in atomic number between the nanoparticles and the support gives rise to high (and directly interpretable) contrast in the image. b) A selection of views taken from an animation of the 3D reconstruction of the object seen in (a). The angle refers to the rotation about a vertical axis.

ing medium. The challenges are to devise a high-tilt-angle stage($\pm 60°$) for the FEG SEM apparatus that is of similar quality to that in the FEG STEM system, and to improve the sensitivity of the BSE detection to discriminate narrower atomic number differences from the support in extended tomographic or topographic analyses. Fortunately, a whole

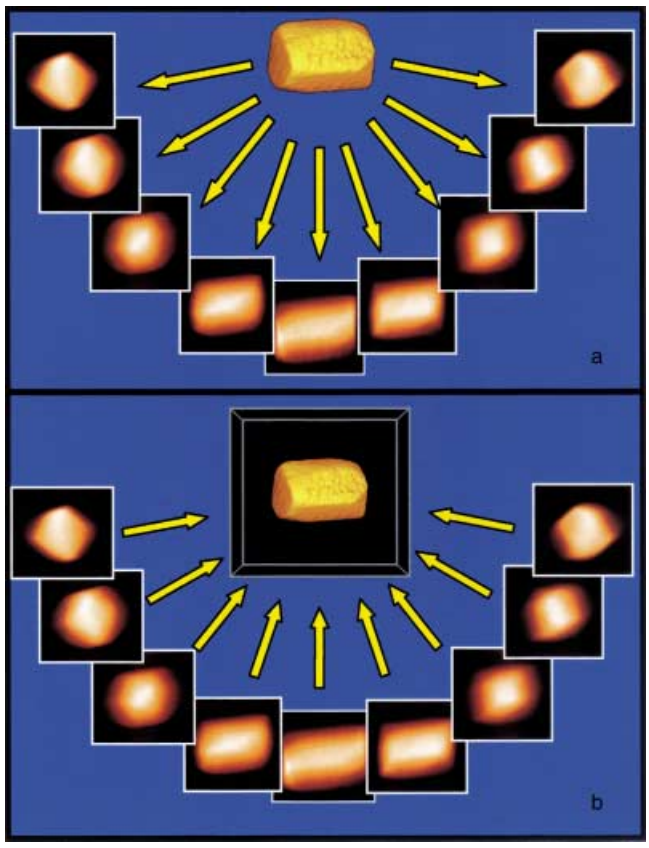

Figure 4. A schematic diagram illustrating a) the acquisition of a series of tilted projections and b) the reconstruction of the 3D object by back-projection (after A. J. Koster[21]). The object is a magnetite nanocrystal from the "backbone" of a magnetotactic bacterium.[31]

class of heterogeneous catalysts are composed of heavier metal particles either in or on a much lighter support. These are particularly suited for both BSE and HAADF imaging because of the similar underlying Rutherford high-angle scattering processes mentioned above. The current data display the considerable potential of the method for chemical and materials science and the possibility of applying the technique to bio-nanomaterials and labeled biomaterials; the latter typically comprising a particle consisting of heavy atoms within a matrix comprised mainly of light atoms.

Received: June 7, 2002 [Z19496]

[1] M. A. El-Sayed, *Acc. Chem. Res.* **2001**, *34*, 257.
[2] H.-G. Boyen, G. Kastle, F. Weigl, P. Ziemann, G. Schmid, M. S. Garner, P. Oelhafen, *Phys. Rev. Lett.* **2001**, *87*, 276401.
[3] P. Stonehart, *J. Appl. Electrochem.* **1992**, *22*, 995.
[4] D. A. Jefferson, J. M. Thomas, G. R. Millward, K. Tsuno, A. Harriman, R. D. Brydson, *Nature* **1986**, *323*, 428.
[5] J. H. Sinfelt, *Bimetallic Catalysts*, Wiley, New York, **1983**.
[6] W. Zhou, J. M. Thomas, D. S. Shephard, B. F. G. Johnson, D. Ozkaya, T. Maschmeyer, R. G. Bell, *Science* **1998**, *280*, 705.
[7] a) T. Ohsuna, O. Terasaki, K. Hiraga, *Mater. Sci. Eng. A* **1996**, *217/218*, 135; b) Y. Horikawa, T. Oshuna, N. Ohnishi, K. Hiraga, O. Terasaki, *Pro. 14th ICEM*, *Electron Microscopy* (Cancun, Mexico), **1998**, p. 385–386.
[8] N. Herron, J. C. Calabrese, W. E. Farreth, Y. Wang, *Science* **1993**, *259*, 1426.
[9] A. E. Hanna, M. Tinkham, *Phys. Rev. B* **1991**, *44*, 5919.

  0044-8249/02/4120-3806 $ 20.00+.50/0

[10] D. Ozkaya, W. Z. Zhou, J. M. Thomas, P. A. Midgley, V. J. Keast, S. Hermans, *Catal. Lett.* **1999**, *60*, 113.
[11] M. M. J. Treacy, A. Howie, *J. Catal.* **1980**, *63*, 265.
[12] P. A. Midgley, M. Weyland, J. M. Thomas, B. F. G. Johnson, *Chem. Commun.* **2001**, *18*, 907–908.
[13] D. S. Shephard, T. Maschmeyer, G. Sankar, J. M. Thomas, D. Ozkaya, B. F. G. Johnson, R. Raja, R. D. Oldroyd, *Eur. J. Chem.* **1998**, *4*, 1214.
[14] A. V. Crewe, J. Wall, J. Longmore, *Science* **1970**, *168*, 1338; M. Isaacson, J. Langmore, N. W. Parker, D. Kopf, M. Utlaut, *Ultramicroscopy* **1976**, *1*, 359.
[15] H. E. Bishop in *X-ray Optics and Microanalysis* (Eds.: R. Castaing, P. Deschamps, J. Philibert), Hermann, Paris, **1966**, p. 153.
[16] K. F. J. Heinrich in *X-ray Optics and Microanalysis* (Eds.: R. Castaing, P. Deschamps, J. Philibert), Hermann, Paris, **1966**, p. 1509.
[17] W. Reuter in *X-ray Optics and Microanalysis* (Eds.: G Shimoda, K. Kohra, T. Ichinokowa), University Tokyo Press, Tokyo, **1972**, p. 121.
[18] E. D. Boyes, *Microsc. Microanal.* **2000**, *6*, 307.
[19] R. A. Crowther, D. J. de Rosier, A. Klug, *Proc. R. Soc. London Ser. A* **1970**, *317*, 319.
[20] J. Frank, *Electron tomography: three-dimensional imaging with the transmission electron microscope*, Plenum, New York, **1992**.
[21] A. J. Koster, U. Ziese, A. J. Verkleij, A. H. Janssen, K. P. de Jong, J. *Phys. Chem. B* **2000**, *104*, 9368.
[22] A. H. Janssen, A. J. Koster, K. P. de Jong, *Angew. Chem.* **2001**, *113*, 1136; *Angew. Chem. Int. Ed.* **2001**, *40*, 1102.
[23] S. R. Deans, *The Radon Transform and Some of Its Applications*, Wiley, New York, **1983**.
[24] P. L. Gai, M. J. Goringe, J. C. Barry, *J. Microsc.* **1986**, *142*, 9.
[25] M. Weyland, PhD thesis, University of Cambridge, **2002**.
[26] A color animation of the reconstruction can be found at www-mem.hrem.cam.ac.uk/research/CETP/Images/Pdanim.gif.
[27] M. Weyland, P. A. Midgley, J. M. Thomas, *J. Phys Chem. B* **2001**, *105*, 7882.
[28] M. Radermacher, *J. Electron Microsc. Tech.* **1988**, *9*, 359.
[29] J. C. Russ, *The Image Processing Handbook*, 3rd ed., IEEE Press, Piscataway, **2000**.
[30] P. Gilbert, *J. Theor. Biol.* **1972**, *36*, 105.
[31] P. R. Buseck, R. E. Dunin-Borkowski, B. Devouard, R. B. Frankel, M. R. McCartney, P. A. Midgley, M. Posfai, M. Weyland, *Proc. Natl. Acad. Sci. USA* **2001**, *98*, 13490.

Methyl Transfer from Rhenium to Coordinated Thiolate Groups**

Xiaopeng Shan, Arkady Ellern, and James H. Espenson*

A prominent reaction of vitamin B_{12} is the conversion of D,L-homocystein, $HS(CH_2)_2CHNH_2CO_2H$, to L-methionine, $MeS(CH_2)_2CHNH_2CO_2H$, with methylcobalamin and methylcobinamide.[1–4] Methyl bis(dimethylglyoximato)cobalt(III) and related complexes also convert thiols to thioethers [Eq. (1)]:[5]

$$Co^{III}-CH_3 + RSH \rightarrow [Co^{I}]^- + RSCH_3 + H^+ \quad (1)$$

There are, however, a lack of precedents in the literature for similar conversions that do not involve organocobalt complexes. In this work, new reactions of rhenium complexes have been examined, and sound evidence for the analogous conversion has now been obtained.

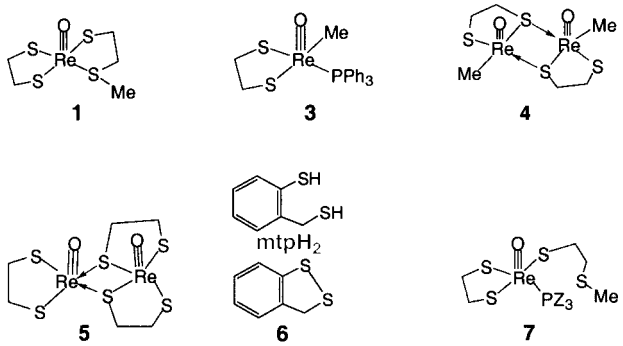

$MeReO_3$ (MTO, **2**)[6] reacts with the readily-oxidized 2-(mercaptomethyl)thiophenol ($mtpH_2$), to yield a disulfide [Eq. (2)]:

$$2\,MeReO_3 + 4\,mtpH_2 \rightarrow \{MeReO(mtp)\}_2\,(\mathbf{4}) + 2\,(\mathbf{6}) + 4\,H_2O \quad (2)$$

With 1,2-ethanedithiol ($edtH_2$), however, a quite different result was obtained. As Re^{VII} was reduced to Re^{V}, one $edtH_2$ molecule was transformed to $HS(CH_2)_2SMe$, which remains coordinated to the rhenium(V) center through both sulfur atoms in a κ^2 fashion [Eq. (3)]:

$$MeReO_3 + 2\,edtH_2 \rightarrow \mathbf{1} + 2\,H_2O \quad (3)$$

Details of the synthesis and characterization of the dark-red complex **1** are given in the Experimental Section. A similar reaction starting with [MeReO(edt)(PPh_3)] (**3**)[7] gave the same product in lower yield. Crystals of **1** suitable for X-ray diffraction could not be obtained. We have formulated the composition of **1** to be [ReO(κ^2-edt)(κ^2-edtMe)] based on elemental analysis and spectroscopic data. An alternative formulation as an organorhenium(VII) compound, [MeReO(edt)$_2$], could not be ruled out by these data. However, the evidence is in favor of structure **1** as the CH_3 resonance appears at $\delta = 1.90$ ppm, which is further downfield than would be expected for a methyl group coordinated to a Re^{VII} center. Indeed, the proposed mechanism suggests that [MeReO(edt)$_2$] lies on the pathway to **1**.

Chemical methods were therefore used to obtain information about the molecular structure of **1**, particularly with respect to whether the Me–Re interaction present in the starting material is retained. The reaction of **1** with H_2O_2 in wet acetonitrile gave ReO_4^- ions, which are easily recognized from the characteristic UV spectrum. The same product was obtained from **5**, another compound that lacks a Me–Re bond. In contrast, several compounds that do contain a Me–Re bond (**2**, **3**, and **4**) cleanly reacted with H_2O_2 to form

[*] Prof. J. H. Espenson, X. Shan, Dr. A. Ellern
Department of Chemistry
Iowa State University
Ames, IA 50011 (USA)
Fax: (+1) 515-294-5233
E-mail: espenson@iastate.edu

[**] This work was supported by the US National Science Foundation, Grant No. CH-9982004. We are grateful to Professor G. M. Miller for a discussion concerning crystallography and to Professor D. J. Darensbourg for the gift of 1,3,5-triaza-phosphaadamantane.

Supporting information for this article is available on the WWW under http://www.angewandte.org or from the author.

  0044-8249/02/4120-3807 $ 20.00+.50/0